Experimental evidence that short-range intermolecular aggregation is sufficient for efficient charge transport in conjugated polymers

Suhao Wang[a], Simone Fabiano[a,1], Scott Himmelberger[b], Skomantas Puzinas[a], Xavier Crispin[a], Alberto Salleo[b], and Magnus Berggren[a]

[a]Laboratory of Organic Electronics, Department of Science and Technology, Linköping University, SE-60174, Norrköping, Sweden; and [b]Department of Materials Science and Engineering, Stanford University, Stanford, CA 94305

Edited by David Ginger, University of Washington, Seattle, WA, and accepted by the Editorial Board July 14, 2015 (received for review January 22, 2015)

Efficiency, current throughput, and speed of electronic devices are to a great extent dictated by charge carrier mobility. The classic approach to impart high carrier mobility to polymeric semiconductors has often relied on the assumption that extensive order and crystallinity are needed. Recently, however, this assumption has been challenged, because high mobility has been reported for semiconducting polymers that exhibit a surprisingly low degree of order. Here, we show that semiconducting polymers can be confined into weakly ordered fibers within an inert polymer matrix without affecting their charge transport properties. In these conditions, the semiconducting polymer chains are inhibited from attaining long-range order in the π-stacking or alkyl-stacking directions, as demonstrated from the absence of significant X-ray diffraction intensity corresponding to these crystallographic directions, yet still remain extended along the backbone direction and aggregate on a local length scale. As a result, the polymer films maintain high mobility even at very low concentrations. Our findings provide a simple picture that clarifies the role of local order and connectivity of domains.

organic electronics | conjugated polymers | aggregation | charge transport

Conjugated polymers have received significant scientific attention as the active material in devices for printed and flexible organic electronics (1, 2). Owing to their versatile chemical synthesis, inexpensive processability from solution, and unique mechanical flexibility, these materials are in fact promising for a vast array of devices in future low-cost and distributed technologies, such as integrated systems for electronic labels targeting safety, security, and surveillance applications (3). The rational design of new organic semiconductors has been guided by a thorough investigation of their limitations in charge transport, leading to the development of high-performance materials for next-generation electronic applications such as low-cost displays, solar cells, sensors, and logic circuits (4, 5). For more than a decade research has primarily focused on increasing the long-range order and the crystallinity of conjugated polymers as a strategy to improve the solid-state charge transport properties. As a result, the charge carrier mobility has increased by several orders of magnitude through the design and synthesis of highly ordered polymers. However, recent studies have suggested that the key to designing high-mobility polymers is not to increase their crystallinity but rather to improve their tolerance for disorder by allowing more efficient intra- and intermolecular charge transport pathways (6). This observation explains why mobility values obtained from recently designed seemingly disordered organic semiconductors often exceed those of polymers having a high degree of crystallinity ($\sim$1 $cm^2 \cdot V^{-1} \cdot s^{-1}$) (7–10). Indeed, polymers may exhibit little long-range order, as measured by X-ray diffraction (XRD), and yet display a remarkable degree of short-range order.

In this respect, poly{[N,N′-bis(2-octyldodecyl)-1,4,5,8-naphthalenediimide-2,6-diyl]-alt-5,5′-(2,2′-bithiophene)} [P(NDI2OD-T2); Scheme 1*A*] (11), an electron-transporting donor-acceptor copolymer, is a very interesting system for studying the structure–property relationships of weakly ordered semiconducting polymers. Indeed, a detailed characterization of this polymer reveals a rather unique solid-state microstructure displaying the simultaneous presence of disordered phases and highly interconnected, fiber-like ordered phases, where the polymer backbones lay preferentially face-on with respect to the substrate (12) and characterized by a dihedral angle between the NDI and thiophene units (13). Whereas a face-on orientation is observed in the bulk of the film, a more edge-on orientation is revealed at the film surface (14, 15). This particular morphology allows good electron transport in both organic diodes and field-effect transistors (OFETs), with high in-plane mobilities of $\sim$0.1–0.6 $cm^2 \cdot V^{-1} \cdot s^{-1}$ even in the presence of a substantial degree of disorder (11). However, film morphologies with predominantly edge-on oriented polymer chains were observed to yield lower performance in both diodes and top-gated OFETs because of the reduced out-of-plane mobility and larger injection barrier (16–19). In a recent publication, Neher and coworkers also showed that this polymer has a strong tendency to aggregate, which greatly affects the bulk optical and electrical properties (20, 21). Control of the preaggregation of this polymer in solution has shown great promise for the optimization of all-polymer solar cells in which P(NDI2OD-T2) is used as a fullerene replacement (22, 23). Although several reports have investigated charge transport of P(NDI2OD-T2) in solution-processed thin films as a function of the processing conditions, the results are often qualitative and a complete description of how charges propagate across the ordered and disordered regions is needed. In particular, the role of aggregation on charge transport in these weakly ordered materials is still poorly understood. To this end, blends of semiconducting and insulating polymers, which allow a

Significance

Understanding the nature of charge transport and its limitations has guided the rational design of organic semiconductors. Research has mainly focused on increasing the crystallinity of conjugated polymers as a strategy to improve the long-range charge transport properties. Here, we demonstrate that local aggregation over very few chains is a sufficient mesoscopic structure to ensure high mobility, with charge transport mainly occurring along the polymer backbones, and that extended crystallinity is not necessary. These results provide an explanation for the high mobilities observed in seemingly disordered polymers and set molecular-design guidelines for next-generation conjugated polymers.

Author contributions: S.F. designed research; S.W., S.F., S.H., and S.P. performed research; S.W., S.F., S.H., and A.S. analyzed data; and S.W., S.F., S.H., X.C., A.S., and M.B. wrote the paper.

The authors declare no conflict of interest.

This article is a PNAS Direct Submission. D.G. is a guest editor invited by the Editorial Board.

[1]To whom correspondence should be addressed. Email: simone.fabiano@liu.se.

This article contains supporting information online at www.pnas.org/lookup/suppl/doi:10.1073/pnas.1501381112/-/DCSupplemental.

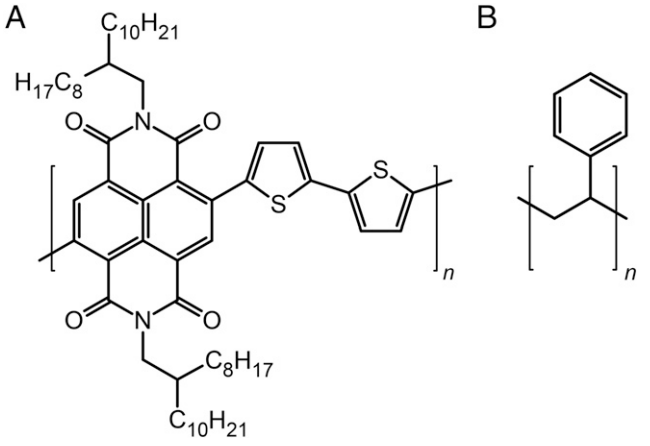

Scheme 1. Chemical structures of (*A*) P(NDI2OD-T2) and (*B*) PS.

fine-tuning of the active layer morphology through confinement, represent a model system for studying the relationship between microstructure and charge transport of semiconducting polymers.

Here, we demonstrate that when P(NDI2OD-T2) is confined into extremely thin layers by an inert polystyrene (PS; Scheme 1*B*) matrix, long-range order is disrupted. Specifically, P(NDI2OD-T2) chains are inhibited from crystallizing over relatively large length scales (π-stacking or alkyl stacking), thus suppressing X-ray diffraction arising from periodicity in those directions, yet still remain extended along the backbone direction. Furthermore, these ultrathin P(NDI2OD-T2) layers retain locally the short-range intermolecular aggregation characteristics of a crystalline film. We make use of these dilute semiconducting blends as a means to uncover the fundamental properties of charge transport in this conjugated polymer. Indeed, by processing the P(NDI2OD-T2) in such a manner, we control the degree of long-range order in the polymer while maintaining the short-range order intact. As a result, we have constructed a model system that allows the systematic investigation of the respective roles of long-range and short-range order on charge transport in conjugated polymers.

It has been shown that charges are confined to crystalline regions of a semicrystalline morphology (6). Owing to the short-range intermolecular aggregation even at very low concentrations, we show that P(NDI2OD-T2) is able to maintain the same mobilities as neat semiconducting films, despite the lack of long-range order. Our findings provide the first direct experimental evidence to our knowledge that local aggregation over very few chains is a sufficient mesoscopic structure to achieve high mobility and that extended crystallinity is not necessary. That is, only local interconnectivity between adjacent domains is sufficient for effective charge transport. These results provide an explanation for the high mobilities observed in weakly diffracting materials and set a guideline for the rational design of next-generation polymers, with the attention being shifted back from a mesoscopic/microstructural level to a molecular level.

Results and Discussion

To study the microstructure of the P(NDI2OD-T2)/PS thin films, grazing incidence X-ray diffraction was performed on a series of blends, composed of 0% to 100% P(NDI2OD-T2) in PS. Characteristic diffraction peaks corresponding to the alkyl-stacking (h00), π-stacking (0k0), and chain backbone (00l) directions were observed in neat films of P(NDI2OD-T2), and two broad rings were observed in disordered PS films (Fig. 1 and Fig. S1). The thin films composed of both polymers showed diffraction features characteristic of each component, respectively, and the crystalline texture of the P(NDI2OD-T2) remained unchanged for all blend ratios (Fig. S2), results that are also consistent with a vertical phase separation (discussed below).

To track the order along the various crystallographic directions as a function of the blend ratio, the integrated intensities of peaks corresponding to each direction were measured and then normalized by the exposure time and volume of P(NDI2OD-T2) in the film (Fig. 2*A*). The normalized alkyl- and π-stacking intensities drop off significantly below a P(NDI2OD-T2) concentration of 40%, to finally completely disappear in films below ∼5% P(NDI2OD-T2). A concurrent decrease in the coherence length (Table 1) is also observed for these two stacking directions, indicating that packing between chains is perturbed as the fraction of P(NDI2OD-T2) in the film is decreased.

In a remarkable contrast, normalized diffraction intensities arising from the chain backbone remain constant across all blend films, even down to concentrations as low as 1% P(NDI2OD-T2). Additionally, the coherence length in the chain backbone direction does not change as a function of P(NDI2OD-T2) content (Table 1). Together, these results indicate that although long-range packing of the chains is severely disrupted when the thickness of the P(NDI2OD-T2) layer drops below ∼10 nm, the relatively rigid P(NDI2OD-T2) chains are still quite extended even in films containing only 1% semiconducting polymer.

Although X-ray results indicate that long-range intermolecular packing is severely disrupted as the P(NDI2OD-T2) content of the blends is reduced, the optical absorption spectra of P(NDI2OD-T2)/PS thin films show the clear presence of aggregation (short-range intermolecular packing) all of the way down to 1% P(NDI2OD-T2) (Fig. 2*B*). P(NDI2OD-T2) has a strong tendency to preaggregate in low-polar solvents, even at low concentrations (20). Similar to what is observed in neat P(NDI2OD-T2) films, aggregation is strongly promoted also for the blends with the formation of aggregate species, exhibiting a main absorption band at ∼710 nm and a shoulder at ∼790 nm (Fig. 2*B*). This structured low-energy absorption represents a clear spectroscopic fingerprint of the formation of aggregate species and was attributed to the interaction of chain segments (20). The optical characteristics of nonaggregate chains are observed only when solvent molecules with large and highly polarizable aromatic cores such as chloronaphthalene are

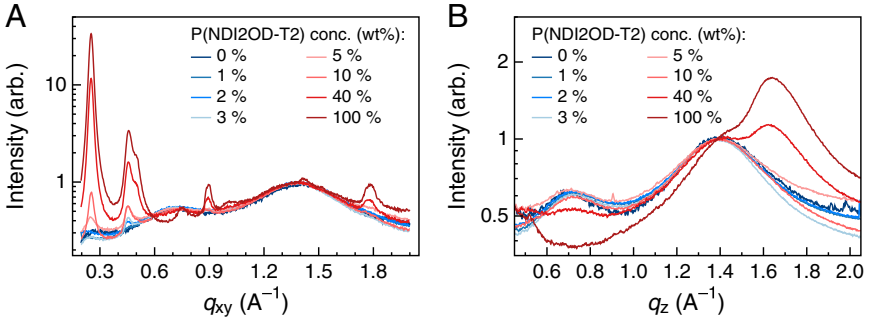

Fig. 1. XRD line cuts for P(NDI2OD-T2)/PS blends along the q_{xy} (*A*) and q_z (*B*) axes. Line cuts have been normalized to the top of the dominant PS peak for visual clarity.

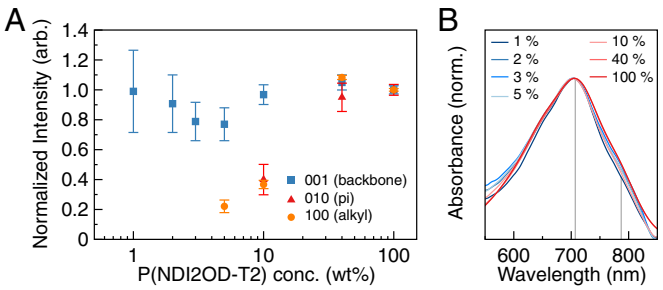

Fig. 2. (*A*) Normalized diffraction intensity of P(NDI2OD-T2) peaks along various crystallographic directions versus P(NDI2OD-T2)/PS blend ratio. Intensities have been normalized for both volume of P(NDI2OD-T2) in the film as well as X-ray exposure time. (*B*) Normalized UV-visible absorption spectra of P(NDI2OD-T2)/PS films with different blend ratios. The gray lines indicate the absorption peaks of the aggregates at ∼710 and ∼790 nm.

used to dissolve the polymer, resulting in unstructured absorption centered at 620 nm. Note that here we have processed the blends from 1,2-dichlorobenzene, a solvent that is known to induce a high degree of preaggregation in the films [∼35% of the P(NDI2OD-T2) total mass] (24). Density functional theory calculations on the optimized structures revealed that this red shift upon aggregation originates mainly from a change in the backbone conformation induced by interchain interactions (20). The persistence in our X-ray measurements of the backbone 001 peaks strongly suggests that the on-chain microstructure of the aggregates is preserved and only the interchain packing is disrupted. Furthermore, by comparing the intensities of the 001 and 002 diffraction peaks, it seems that the 001 peak is always more intense than the 002, suggesting that these aggregates consist mainly of chains with a segregated structure where the donor (acceptor) units stack on top of each other (25). Mixed structures with donor units stacking on top of acceptor units of adjacent chains would in fact exhibit a suppressed 001 diffraction (24).

Neher and coworkers (24) also observed a strict linear correlation between the (001) coherence length associated with the average length of straight-chain segments and the degree of aggregation originating from the planarization of the P(NDI2OD-T2) backbone upon interchain interactions. This correlation exists because interchain interactions enforce a linear chain conformation, thus extending the conjugation length. In the present study, we observed that diluted and neat P(NDI2OD-T2) film show the same degree of aggregation as indicated by a nearly identical low-energy vibronic progression (Fig. 2*B*). In view of the fact that the low-energy band ascribed to aggregates is determined by the length of straight chain segments, the observed correlation demonstrates that the single-chain conformation of P(NDI2OD-T2) in both concentrated and dilute films is similar. This observation is also corroborated by a nearly constant backbone (001) coherence length observed in our case when going from 100% down to 1% P(NDI2OD-T2) films (Fig. 2*A*). This apparent contradiction between the X-ray and optical results is reconciled by the fact that X-ray diffraction relies on constructive interference arising from multiple repeat units in a particular crystallographic direction, whereas aggregate absorption features due to intermolecular interactions can result from aggregates comprising as few as two chains (26). Although long-range crystallinity is disrupted in films including diluted contents of P(NDI2OD-T2), chains are still able to aggregate into local domains, such that they exhibit optical features due to aggregation. In summary, the diluted P(NDI2OD-T2) film can exhibit the X-ray diffraction of a highly disordered material and yet retain virtually the same local aggregation characteristics of a crystalline neat conjugated polymer film, thereby demonstrating the relative importance of short- and long-range order in microstructure characterization and transport.

Atomic force microscopy (AFM) allows for a closer view of the top layer morphology for the different P(NDI2OD-T2)/PS ratios (Fig. 3). Although no obvious features can be observed in the height images (Fig. S3), phase-separated structures composed of P(NDI2OD-T2) and PS can be clearly identified in the phase images down to 1% P(NDI2OD-T2) content. For P(NDI2OD-T2)/PS blends spin-coated on SiO_2, most of the P(NDI2OD-T2) is accumulated at the topmost part of the film. This observation is confirmed by depth-dependent X-ray photoelectron spectroscopy measurements which show the concentrations of nitrogen, oxygen, and sulfur [elements found in P(NDI2OD-T2)] to be enriched near the surface of the film (Fig. S4). Such vertical phase separation featuring a P(NDI2OD-T2)-rich top layer and a bottom interface primarily composed of PS is attributed to the different surface energies of P(NDI2OD-T2) and PS. Indeed, P(NDI2OD-T2) with a low surface energy (23.7 $mJ{\cdot}m^{-2}$; ref. 23) tends to segregate at the air/film interface, whereas PS with higher surface energy (40.2 $mJ{\cdot}m^{-2}$; ref. 27) prefers the SiO_2 surface. A similar surface-induced phase separation is typically reported for other semiconductor/insulator polymer blends (28–30). A characteristic single-phase morphology with randomly oriented crystalline grains on the order of 10–30 nm is observed in neat films of P(NDI2OD-T2) (Fig. 3*A* and Fig. S3*A*). Decreasing the concentration of P(NDI2OD-T2) in the blends results in extended P(NDI2OD-T2) fibers, stretching over micrometer-long distances (Fig. 3 *D* and *E*). Our results are consistent with a similar long-range organization, with the polymer backbones extending over micrometer length-scales, which has been recently revealed for neat films of P(NDI2OD-T2) by high-resolution transmission electron microscopy (31). These results are in agreement with the constant chain backbone coherence length observed by XRD, suggesting that P(NDI2OD-T2) chains are equally extended along the backbone/fiber direction for all blends. Although the exact cause of the drop in alkyl- and π-stacking coherence lengths is

Table 1. Crystalline coherence length of P(NDI2OD-T2) peaks along various crystallographic directions and OFET performance for different P(NDI2OD-T2)/PS blend ratios

P(NDI2OD-T2) concentration, wt%	L_c (001), nm	L_c (100), nm	L_c (010), nm	PTrFE		CYTOP
				μe,* $cm^2{\cdot}V^{-1}{\cdot}s^{-1}$	μh,* $cm^2{\cdot}V^{-1}{\cdot}s^{-1}$	μe,* $cm^2{\cdot}V^{-1}{\cdot}s^{-1}$
100	17.5	25.1	2.0	2.2 (± 0.2) ×10^{-2}	8.1 (± 1.8) ×10^{-3}	3.0 (± 0.3) ×10^{-1}
40	18.5	25.1	2.0	—	—	—
10	17.5	18.5	1.5	1.7 (± 0.4) ×10^{-2}	7.6 (± 0.5) ×10^{-3}	1.3 (± 0.5) ×10^{-1}
5	18.5	9.1	—	9.0 (± 3.3) ×10^{-2}	2.7 (± 1.2) ×10^{-2}	1.3 (± 0.6) ×10^{-1}
3	20.3	—	—	1.0 (± 0.3) ×10^{-1}	1.9 (± 0.8) ×10^{-2}	1.0 (± 0.2) ×10^{-1}
2	17.0	—	—	5.3 (± 0.8) ×10^{-2}	1.0 (± 0.3) ×10^{-2}	1.1 (± 0.3) ×10^{-1}
1	16.5	—	—	2.7 (± 2.2) ×10^{-2}	0.7 (± 0.6) ×10^{-2}	0.4 (± 0.2) ×10^{-1}

*The OFET mobilities were calculated in the saturation regime ($|V_{DS}| = 60$ V) and normalized for the coverage area, as extracted by AFM image thresholding method.

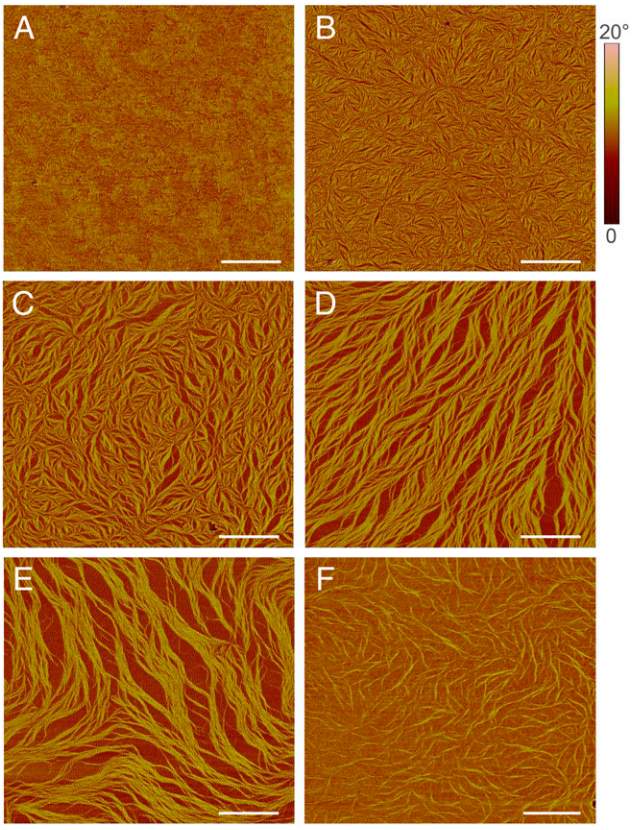

Fig. 3. Tapping-mode AFM phase images of P(NDI2OD-T2)/PS films with different blend ratios: (*A*) neat P(NDI2OD-T2), (*B*) 10%, (*C*) 5%, (*D*) 3%, (*E*) 2%, and (*F*) 1% P(NDI2OD-T2). (Scale bars, 1 μm.)

difficult to determine, adjacent fibers that are coherent in concentrated samples may no longer be so in the dilute blends. The fibers become more dispersed in lower concentration films and at a P(NDI2OD-T2) content of 1%, the AFM phase image shows poorly interconnected P(NDI2OD-T2) fibers embedded in the PS matrix (Fig. 3*F*). The morphologies are isotropic over the macroscopic areas used for charge transport and XRD measurements (Fig. S5).

To directly assess the impact of the reported nano-/microscale morphologies on the charge transport properties of the P(NDI2OD-T2)/PS blend, we fabricated top-gate/bottom-contact OFETs. A detailed description of the fabrication process is given in *Materials and Methods*. It should be noted that P(NDI2OD-T2) is a typical high-mobility n-type semiconductor with a low degree of energetic disorder (32) and both theoretical and experimental studies have shown intrinsically unbalanced electron and hole transport properties in low (i.e., diodes) and high (i.e., OFETs) charge density regimes (33). However, when fluorinated, high-k gate polymers are used as a dielectric insulator, both electrons and holes can be accumulated in the channel, leading to balanced ambipolarity (34, 35). The dielectric used here is a 600-nm-thick poly(trifluoroethylene) (PTrFE) film. Such a high-k, fluorinated gate dielectric can be dissolved in solvents that are perfectly orthogonal to the underlying semiconductor/insulator polymer blend, preventing the latter from rinsing off during deposition of the dielectric. Fig. 4 shows representative transfer characteristics of a P(NDI2OD-T2)/PS OFET containing 3% P(NDI2OD-T2). The transistors exhibit hysteresis-free ambipolar characteristics with a large on/off ratio of $\sim 10^4$. Similar ambipolar transfer characteristics are in fact observed for all of the P(NDI2OD-T2)/PS-based OFETs including channels of different blend ratios (Fig. S6). The average saturation mobility shows a maximum value for the 3–5% P(NDI2OD-T2) content films (average mobility ~0.09 $cm^2 \cdot V^{-1} \cdot s^{-1}$ for electrons and ~0.02 $cm^2 \cdot V^{-1} \cdot s^{-1}$ for holes, as extracted from the transfer characteristics at $|V_{DS}| = 60$ V). The measured electron mobility compares favorably with previously reported P(NDI2OD-T2)-based OFETs using conventional low-k polymers as the dielectric insulator, if one takes into account the well-known lowering of charge mobility that is due to the energetic disorder induced by high-k dielectrics (36). Indeed, when the low-k poly(perfluoroalkenylvinyl ether) (CYTOP) is used as the dielectric, a higher electron mobility is observed (Fig. S7). Note that when normalized for the effective coverage of the channel, as extracted by an AFM image thresholding method, the mobility is found to be invariant regardless of the P(NDI2OD-T2) concentration (Fig. 4*B* and Table 1). The large mobility variation observed for 1% P(NDI2OD-T2) OFETs is most likely due to the poorly interconnected P(NDI2OD-T2) fibers as observed by AFM analysis. No charge transport was observed for 40% P(NDI2OD-T2) OFETs, most likely due to lateral phase separation of the polymer blend as observed by AFM (Fig. S8).

It is noteworthy that although the X-ray results indicate that long-range intermolecular packing is severely disrupted in films of low P(NDI2OD-T2) content, the charge carrier mobility remains high. Noriega et al. (6) have posited that many of the newly developed donor–acceptor polymers are able to maintain a high charge carrier mobility despite low levels of crystallinity, as inferred by X-ray diffraction, owing to their ability to form interconnected aggregates, which allow for efficient intermolecular charge transport. In the system studied here, this seems to be the case. As the fraction of P(NDI2OD-T2) in the film is decreased, long-range order is disrupted due to the confined nature of the semiconducting molecules. However, P(NDI2OD-T2) chains remain extended, well connected, and are still able to locally aggregate as well as in neat films even at concentrations as low as 1%. Thus, these films are able to maintain a high mobility despite the lack of long-range crystallographic order. Although high-performance blends of

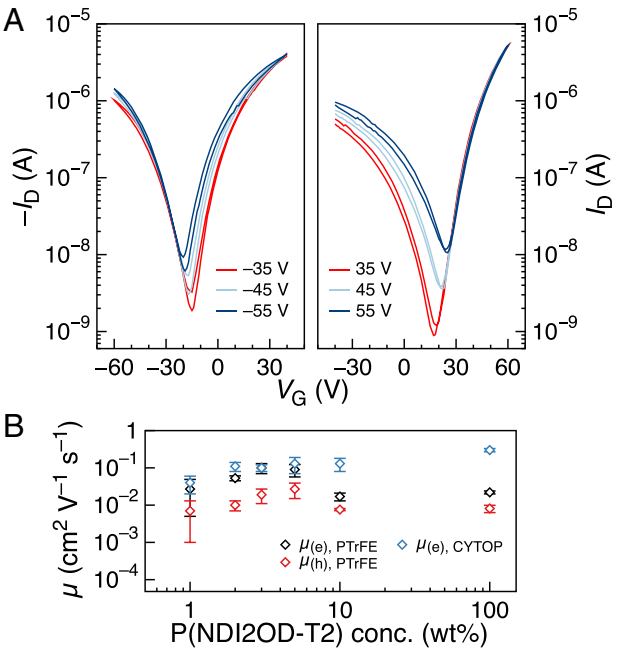

Fig. 4. (*A*) Representative transfer curves of a P(NDI2OD-T2)/PS-based OFET containing 3% P(NDI2OD-T2) and PTrFE as the gate dielectric. The channel length (*L*) and width (*W*) are 30 μm and 500 μm, respectively. (*B*) Dependence of the electron/hole mobility (calculated at $|V_{DS}| = 60$ V and normalized for the coverage area, as extracted by AFM image thresholding method) on the P(NDI2OD-T2)/PS blend ratio.

diluted conjugated polymers with commodity polymers have been reported over the last 10 y (28–30), here we make use of these blends as a tool to independently control the degree of long-range and short-range order and provide unique experimental evidence that high charge carrier mobility can be maintained despite the complete absence of long-range interchain order (i.e., well-defined XRD peaks). In fact, our findings are in contrast with what has been previously reported for blends of insulating and semicrystalline polymers, such as for example poly(3-hexylthiophene), where a significant long-range crystallinity is still observed in the high-performing films even at low concentration of conjugated polymers.

Having demonstrated well-balanced, high-performance ambipolar OFETs containing only 3% P(NDI2OD-T2), we fabricated complementary-like [i.e., complementary metal–oxide–semiconductor (CMOS)-like] inverters as depicted in Fig. S9. In particular, the inverters show an ideal switching characteristic with an inversion voltage close to half the supply voltage (V_{DD}), that is, at $\sim 1/2V_{DD} = 35$ V, a high voltage gain of ~65, and a high noise margin of 67% of the theoretical maximum value of $1/2V_{DD}$ due to the balanced ambipolar transport. High gains (>30) are observed for inverters with just 2% P(NDI2OD-T2) in the blend (Fig. S10). To the best of our knowledge these values are among the best ever reported for solution-processed organic CMOS-like inverters (37).

Conclusions

In conclusion, we demonstrated that the long-range order of P(NDI2OD-T2) can be tuned without affecting the charge transport properties of this material. More specifically, we showed that when P(NDI2OD-T2) is confined within an inert polymer matrix into extremely thin layers, the long-range crystallinity (π-stacking or alkyl stacking) is disrupted whereas short-range aggregation is unperturbed. However, P(NDI2OD-T2) chains still remain extended along the backbone direction, thus maintaining high mobilities by enabling an efficient connection between aggregates. When implemented in CMOS-like inverters, these inexpensive polymer blends yield remarkably high performances, allowing the fabrication of cheap digital logic technologies. These results provide a simple picture that clarifies the role of local order and connectivity: Significantly higher carrier mobilities should be achievable through simultaneous improvements of the local aggregation and interconnectivity of domains. The successful integration of these properties correlates with the remarkable transport properties of the polymer and serves as a guideline for the rational design of next-generation polymers. Research should be shifted to the molecular level with a focus on the interchain coupling in the aggregates and/or the design of molecules that afford delocalization and minimize trapping (38).

Materials and Methods

OFET Device Fabrication. Corning Eagle 2000 glass substrates were cleaned sequentially in water, acetone, and isopropanol for 10 min each, following by drying with nitrogen. Source-drain electrodes patterns were fabricated using a conventional evaporation procedure through metal shadow mask (channel length 30 μm, channel width 500 μm). Five-nanometer-thick Ti was used as adhesion layer of the Au electrodes on glass. The semiconducting polymer P(NDI2OD-T2) (ActivInk N2200; Polyera Inc.) and PS (molecular weight 100 kDa; Aldrich) were separately dissolved in 1,2-dichlorobenzene, both at the concentration of 8 mg/mL. P(NDI2OD-T2)/PS solutions were obtained by mixing the two above-mentioned solutions in volume ratios. Before film deposition, both polymer solutions were stirred for at least 2 h to allow complete dissolution of the samples. After stirring, the solutions were spin-coated onto the glass substrates at 1,000 rpm for 90 s. Then, the films were thermally annealed at 120 °C under nitrogen atmosphere for 10 min and cooled down to room temperature naturally. The dielectric polymer PTrFE (Solvay SA) was dissolved in acetonitrile to form a 60 mg/mL solution, then spin-coated on top of the P(NDI2OD-T2)/PS films at 2,000 rpm for 60 s. After the dielectric layers were deposited, the devices were baked at 80 °C under nitrogen atmosphere for 30 min and cooled down to room temperature. The perfluorinated polymer CYTOP CTL-809M dielectric (Asahi Glass) was spun as received at 6,000 rpm in air, yielding a dielectric thickness of 500–600 nm. After the CYTOP deposition, the devices were annealed under nitrogen, on a hot plate, at 110 °C for 5 h. Finally, the devices were completed by evaporating a 70-nm-thick Al gate electrode through a metal shadow mask on top of the dielectric layers.

Thin Film and OFET Device Characterization. Atomic force microscopy (Nanoscope IIIa AFM; Digital Instruments) was operated in tapping mode to characterize the surface morphologies. UV-absorption spectra were recorded using a UV-visible spectrophotometer (CARY-5000; Varian). All of the OFET electrical characteristics were measured using a Keithley 4200-SCS in air.

XRD Measurements. All measurements were performed at the Stanford Synchrotron Radiation Lightsource on beamline 11-3. The incident X-ray beam was set at a grazing incidence (0.12°), which was chosen to be above the critical angle of the polymer film but below that of the silicon substrate, ensuring that the full thickness of the film was sampled. Samples were kept in a helium-filled environment during the measurements. Diffraction data analysis was performed with the software WxDiff and coherence lengths were calculated using the Scherrer equation.

ACKNOWLEDGMENTS. This research was partially supported by the Advanced Functional Materials Center at Linköping University and the Önnesjö Foundation. The authors thank the Knut and Alice Wallenberg Foundation (Power Paper project, scholars), the Swedish Foundation for Strategic Research (Synergy project), and the Swedish Governmental Agency for Innovation Systems (VINNOVA) for financial support. This work was also supported by National Science Foundation Grant DMR 1205752 (to A.S. and S.H.). Use of the Stanford Synchrotron Radiation Lightsource, SLAC National Accelerator Laboratory, is supported by the US Department of Energy, Office of Science, Office of Basic Energy Sciences under Contract DE-AC02-76SF00515.

1. Arias AC, MacKenzie JD, McCulloch I, Rivnay J, Salleo A (2010) Materials and applications for large area electronics: Solution-based approaches. *Chem Rev* 110(1):3–24.
2. Facchetti A (2011) π-Conjugated polymers for organic electronics and photovoltaic cell applications. *Chem Mater* 23(3):733–758.
3. Berggren M, Nilsson D, Robinson ND (2007) Organic materials for printed electronics. *Nat Mater* 6(1):3–5.
4. Gelinck GH, et al. (2004) Flexible active-matrix displays and shift registers based on solution-processed organic transistors. *Nat Mater* 3(2):106–110.
5. Kronemeijer AJ, et al. (2012) A selenophene-based low-bandgap donor-acceptor polymer leading to fast ambipolar logic. *Adv Mater* 24(12):1558–1565.
6. Noriega R, et al. (2013) A general relationship between disorder, aggregation and charge transport in conjugated polymers. *Nat Mater* 12(11):1038–1044.
7. Bronstein H, et al. (2011) Thieno[3,2-b]thiophene-diketopyrrolopyrrole-containing polymers for high-performance organic field-effect transistors and organic photovoltaic devices. *J Am Chem Soc* 133(10):3272–3275.
8. Mei J, Kim H, Ayzner AL, Toney MF, Bao Z (2011) Siloxane-terminated solubilizing side chains: Bringing conjugated polymer backbones closer and boosting hole mobilities in thin-film transistors. *J Am Chem Soc* 133(50):20130–20133.
9. Tsao HN, et al. (2011) Ultrahigh mobility in polymer field-effect transistors by design. *J Am Chem Soc* 133(8):2605–2612.
10. Zhang X, et al. (2013) Molecular origin of high field-effect mobility in an indacenodithiophene-benzothiadiazole copolymer. *Nat Commun* 4:2238.
11. Yan H, et al. (2009) A high-mobility electron-transporting polymer for printed transistors. *Nature* 457(7230):679–686.
12. Rivnay J, et al. (2010) Unconventional face-on texture and exceptional in-plane order of a high mobility n-type polymer. *Adv Mater* 22(39):4359–4363.
13. Giussani E, Fazzi D, Brambilla L, Caironi M, Castiglioni C (2013) Molecular level investigation of the film structure of a high electron mobility copolymer via vibrational spectroscopy. *Macromolecules* 46(7):2658–2670.
14. Collins BA, et al. (2012) Polarized X-ray scattering reveals non-crystalline orientational ordering in organic films. *Nat Mater* 11(6):536–543.
15. Schuettfort T, Thomsen L, McNeill CR (2013) Observation of a distinct surface molecular orientation in films of a high mobility conjugated polymer. *J Am Chem Soc* 135(3):1092–1101.
16. Schuettfort T, et al. (2011) Surface and bulk structural characterization of a high-mobility electron-transporting polymer. *Macromolecules* 44(6):1530–1539.
17. Rivnay J, et al. (2011) Drastic control of texture in a high performance n-type polymeric semiconductor and implications for charge transport. *Macromolecules* 44(13):5246–5255.
18. Fabiano S, et al. (2012) From monolayer to multilayer N-channel polymeric field-effect transistors with precise conformational order. *Adv Mater* 24(7):951–956.
19. Fabiano S, Yoshida H, Chen Z, Facchetti A, Loi MA (2013) Orientation-dependent electronic structures and charge transport mechanisms in ultrathin polymeric n-channel field-effect transistors. *ACS Appl Mater Interfaces* 5(10):4417–4422.

20. Steyrleuthner R, et al. (2012) Aggregation in a high-mobility n-type low-bandgap copolymer with implications on semicrystalline morphology. *J Am Chem Soc* 134(44): 18303–18317.
21. Luzio A, Criante L, D'Innocenzo V, Caironi M (2013) Control of charge transport in a semiconducting copolymer by solvent-induced long-range order. *Sci Rep* 3:3425.
22. Schubert M, et al. (2012) Influence of aggregation on the performance of all-polymer solar cells containing low-bandgap naphthalenediimide copolymers. *Adv Energy Mater* 2(3):369–380.
23. Fabiano S, et al. (2014) Charge transport orthogonality in all-polymer blend transistors, diodes, and solar cells. *Adv Energy Mater* 4(6):1301409.
24. Steyrleuthner R, et al. (2014) The role of regioregularity, crystallinity, and chain orientation on electron transport in a high-mobility n-type copolymer. *J Am Chem Soc* 136(11):4245–4256.
25. Brinkmann M, et al. (2012) Segregated versus mixed interchain stacking in highly oriented films of naphthalene diimide bithiophene copolymers. *ACS Nano* 6(11): 10319–10326.
26. Duong DT, Toney MF, Salleo A (2012) Role of confinement and aggregation in charge transport in semicrystalline polythiophene thin films. *Phys Rev B* 86(20):205205.
27. Tanaka K, Takahara A, Kajiyama T (1996) Film thickness dependence of the surface structure of immiscible polystyrene/poly(methyl methacrylate) blends. *Macromolecules* 29(9):3232–3239.
28. Lu G, et al. (2013) Moderate doping leads to high performance of semiconductor/insulator polymer blend transistors. *Nat Commun* 4:1588.
29. Goffri S, et al. (2006) Multicomponent semiconducting polymer systems with low crystallization-induced percolation threshold. *Nat Mater* 5(12):950–956.
30. Qiu L, et al. (2009) Organic thin-film transistors based on polythiophene nanowires embedded in insulating polymer. *Adv Mater* 21(13):1349–1353.
31. Takacs CJ, et al. (2013) Remarkable order of a high-performance polymer. *Nano Lett* 13(6):2522–2527.
32. Caironi M, et al. (2011) Very low degree of energetic disorder as the origin of high mobility in an n-channel polymer semiconductor. *Adv Funct Mater* 21(17):3371–3381.
33. Wetzelaer G, et al. (2012) Asymmetric electron and hole transport in a high-mobility n-type conjugated polymer. *Phys Rev B* 86:165203.
34. Baeg KJ, et al. (2012) Remarkable enhancement of hole transport in top-gated N-type polymer field-effect transistors by a high-k dielectric for ambipolar electronic circuits. *Adv Mater* 24(40):5433–5439.
35. Fabiano S, et al. (2014) Selective remanent ambipolar charge transport in polymeric field-effect transistors for high-performance logic circuits fabricated in ambient. *Adv Mater* 26(44):7438–7443.
36. Veres J, Ogier SD, Leeming SW, Cupertino DC, Mohialdin Khaffaf S (2003) Low-k insulators as the choice of dielectrics in organic field-effect transistors. *Adv Funct Mater* 13(3):199–204.
37. Baeg KJ, Caironi M, Noh YY (2013) Toward printed integrated circuits based on unipolar or ambipolar polymer semiconductors. *Adv Mater* 25(31):4210–4244.
38. Fornari RP, Troisi A (2014) Narrower bands with better charge transport: The counterintuitive behavior of semiconducting copolymers. *Adv Mater* 26(45):7627–7631.